

Minimum-Fuel Powered Descent for Mars Pinpoint Landing

Ufuk Topcu,* Jordi Casoliva,† and Kenneth D. Mease‡
University of California, Irvine, California 92697-3975

DOI: 10.2514/1.25023

Motivated by the requirement for pinpoint landing in future Mars missions, we consider the problem of minimum-fuel powered terminal descent to a prescribed landing site. The first-order necessary conditions are derived and interpreted for a point-mass model with throttle and thrust angle control and for rigid-body model with throttle and angular velocity control, clarifying the characteristics of the minimum-fuel solution in each case. The optimal thrust magnitude profile is bang–bang for both models; for the point-mass, the most general thrust magnitude profile has a maximum–minimum–maximum structure. The optimal thrust direction law for the point-mass model (alignment with the primer vector) corresponds to a singular solution for the rigid-body model. Whether the point-mass solution accurately approximates the rigid-body solution depends on the thrust direction boundary conditions imposed for the rigid-body model. Minimum-fuel solutions, obtained numerically, illustrate the optimal strategies.

Nomenclature

C	=	characteristic velocity, m/s
\mathbf{g}	=	gravitational acceleration vector, m/s ²
g_E	=	gravitational acceleration at the Earth's surface, m/s ²
H	=	Hamiltonian
h	=	altitude, m
I_{sp}	=	specific impulse of the engines, s
J	=	cost function, m/s
k	=	inverse of the ejection velocity, (m/s) ⁻¹
m	=	lander mass, kg
\mathbf{r}	=	lander position vector, m
\mathbf{T}	=	thrust vector, N
t	=	time, s
u	=	downrange velocity coordinate, m/s
\mathbf{V}	=	lander velocity vector, m/s
v	=	crossrange velocity coordinate, m/s
v_e	=	ejection velocity of the engines, m/s
w	=	vertical velocity coordinate, m/s
x	=	downrange position coordinate, m
y	=	crossrange position coordinate, m
β	=	cant angle for the engines, rad
$\mathbf{\Gamma}$	=	specific thrust vector, N/kg
θ	=	pitch angle, rad
λ	=	costate variable
ν	=	yaw angular velocity, rad/s
ψ	=	yaw angle, rad
ω	=	pitch angular velocity, rad/s

Subscripts

f	=	final condition
0	=	initial condition

Presented as Paper 6286 at the AIAA Guidance, Navigation, and Control Conference and Exhibit, San Francisco, CA, 15–18 August 2005; received 7 May 2006; revision received 15 December 2006; accepted for publication 9 January 2007. Copyright © 2007 by the authors. Published by the American Institute of Aeronautics and Astronautics, Inc., with permission. Copies of this paper may be made for personal or internal use, on condition that the copier pay the \$10.00 per-copy fee to the Copyright Clearance Center, Inc., 222 Rosewood Drive, Danvers, MA 01923; include the code 0022-4650/07 \$10.00 in correspondence with the CCC.

*Graduate Student Researcher, Department of Mechanical and Aerospace Engineering; Currently Graduate Student Researcher, Department of Mechanical Engineering, University of California, Berkeley.

†Graduate Student Researcher, Department of Mechanical and Aerospace Engineering.

‡Professor, Department of Mechanical and Aerospace Engineering, Associate Fellow AIAA.

Introduction

MARS pinpoint landing (defined as landing within 100 m of a selected surface location) is a potential requirement for future Mars missions [1]. Our focus in this paper is on the powered descent phase which commences once the subsonic parachute has reduced the lander velocity to 55–90 m/s and is jettisoned [1]. During the terminal powered descent phase, in addition to achieving a soft landing, it may be necessary to translate horizontally as much as several kilometers to compensate for drift due to the effects of unpredictable winds during the parachute phase. Fuel-efficient powered descent guidance is important to keep the lander mass as low as possible.

The powered descent guidance currently baselined for the Mars Science Laboratory (MSL) lander [2] is a derivative of the Apollo lunar descent guidance [3]. In both of these schemes, the vehicle position, velocity, and acceleration variables are represented by consistent polynomial functions of time with just enough free parameters to meet the boundary conditions. Comparison [4] of the feasible solution generated by this approach, with the minimum-fuel solution, indicates significantly greater propellant consumption when lateral flight of several kilometers is required,[§] motivating the development of alternative guidance algorithms that are more fuel efficient. In designing a fuel-efficient guidance algorithm, it is useful to know the control strategy that minimizes the fuel consumption. To accommodate operational constraints and additional guidance problem features, a different control strategy might be used in a guidance algorithm, but still, an understanding of the minimum-fuel solution can aid the algorithm design and serve as a standard for performance evaluation. Several candidate guidance algorithms have already been proposed [5–7].

The purposes of this paper are 1) to formulate the three-dimensional minimum-fuel problem for the powered terminal descent of a Mars lander, 2) to derive and interpret the first-order necessary conditions, and 3) to obtain minimum-fuel solutions that illustrate the optimal strategy. Both a point-mass model with throttle and thrust angle control and a rigid-body model with throttle and angular velocity control are considered. The rigid-body model with angular velocity control allows us to consider the effects of boundary conditions on the thrust direction and finite bounds on the angular velocities. The theoretical results are derived in a self-contained manner. Some of the results were first derived in the period 1950–1970, the formative years of optimal control and its application to flight mechanics. In the next paragraph, we mention some key references that are relevant and that provide links to pioneering and foundational work carried out in that era. Specific credit for results will also be given during the course of our derivations in the body of the paper.

[§]Neither Apollo nor MSL had this requirement.

The general theory for minimum-fuel trajectories in a uniform gravitational field is presented by Lawden [8], Miele [9], Leitmann [10], and Marec [11]. Two-dimensional powered-flight for a point-mass model with bounded thrust was considered by Leitmann [10,12]. He showed that the optimal thrust magnitude profile is composed of maximum and minimum arcs, and there are at most three arcs. He proved that the use of intermediate thrust levels, corresponding to a singular arc, is not optimal. Kelley [13] considered optimal powered-flight for the rigid-body model with torque control as a two-timescale singular perturbation problem. When the optimal solution is of the two-timescale boundary-layer type, he showed that the solution is similar to that for the point-mass model except for initial and final boundary layers where the solution is modified to satisfy the boundary conditions.

The contributions of this paper are 1) an analytical treatment of the point-mass and rigid-body models in one place, with a more complete analysis of the rigid-body case than previously available, 2) the similarities and differences between the point-mass and rigid-body solutions, and the factors affecting them, are identified, and 3) computation of numerical solutions that illustrate the specific minimum-fuel descents. With the computational power available today, optimal trajectory studies are often carried out with numerical methods alone. The minimum-fuel landing problem is one for which analytical methods uncover the general qualitative characteristics of the optimal solutions and complement the quantitative information provided by numerical solutions for particular boundary conditions. Although the motivation for this study and the data for the numerical results concern Mars landing, the results are more generally applicable, for example, to lunar landing.

Powered Descent Modeling

Characteristic Velocity

The rate of change of mass, due to propellant consumption, is

$$\dot{m} = -kT \quad (1)$$

where $k = v_e^{-1}$ and T is the thrust magnitude. We assume constant ejection velocity. The ejection velocity is related to the specific impulse of the engines by $v_e = g_E I_{sp}$. Following Marec[11], we will use characteristic velocity instead of mass as a state variable in deriving the necessary conditions. The characteristic velocity is defined as the solution to the equation

$$\dot{C} = \Gamma \quad (2)$$

with initial condition $C(t_0) = 0$, where $\Gamma = T/m$ is the magnitude of the specific thrust. There are constant upper and lower bounds on the thrust force that translate to time-varying upper and lower bounds on the thrust acceleration, expressed as

$$0 \leq \Gamma_{\min}(t) \leq \Gamma(t) \leq \Gamma_{\max}(t) \quad (3)$$

The time dependence of the bounds is due to the mass variation. Given $C(t)$, the corresponding mass is $m(t) = m(t_0) \exp[-kC(t)]$, $\Gamma_{\min}(t) = T_{\min}/m(t)$, and $\Gamma_{\max}(t) = T_{\max}/m(t)$. Thus, the bounds should be viewed as C dependent, when C is used in place of m as a state variable. To convert bounds on thrust force to bounds on thrust acceleration, the initial mass of the vehicle and propellant and the engine I_{sp} are needed. For the numerical solutions presented later, the mass is used in place of C and thrust force is the control.

Vehicle Dynamics

The dynamics for the translational degrees of freedom and the characteristic velocity are

$$\dot{\mathbf{r}} = \mathbf{V} \quad \dot{\mathbf{V}} = \mathbf{g} + \mathbf{\Gamma} \quad \dot{C} = \Gamma \quad (4)$$

When Γ is written without the bold/italic font, it denotes the scalar magnitude of the vector $\mathbf{\Gamma}$, and this convention will be used for other vectors as well. Defining \mathbf{D} as a unit vector in the thrust direction, we can express the thrust vector by $\mathbf{\Gamma} = \Gamma \mathbf{D}$.

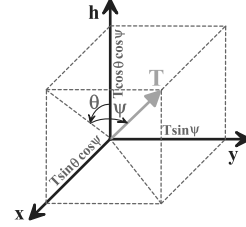


Fig. 1 The thrust vector and its components in the x, y , and h axes.

It is assumed that the gravitational field is uniform, i.e., that \mathbf{g} is constant, and that aerodynamic forces can be neglected. Further, we assume $0 \leq \Gamma_{\min}(t) < g < \Gamma_{\max}(t)$ for all t within the time interval of interest. Assuming $\Gamma_{\max} > g$, or equivalently a thrust-to-weight ratio greater than one, is generally required to achieve a soft landing. Specifically, we will impose the condition that the vertical velocity is zero when the surface is reached; positive vertical acceleration is required to go from the negative vertical velocity in descent to zero vertical velocity. The case $0 \leq \Gamma_{\min}(t) < g$ is the most natural. Ideally Γ_{\min} corresponds to thrust off and would in this case be zero. However, it may not be possible, or at least safe, to throttle the engines down to zero if thrust will be needed subsequently. Thus, we leave some freedom in Γ_{\min} . For the numerical results presented later Γ_{\min} corresponds to 30% throttle. The upper bound $\Gamma_{\max} < g$ is not necessary for any of the theoretical results presented in this paper.

The position and velocity vectors are expressed in Cartesian coordinates for the purpose of obtaining numerical solutions. The position vector coordinates are (x, y, h) as shown in Fig. 1. The desired landing site is at the origin. The x axis is directed such that the initial vehicle position has $x > 0$ and $y = 0$. We assume this coordinate frame is inertial. The velocity coordinates are $(u, v, w)^T = (\dot{x}, \dot{y}, \dot{h})^T$. The direction of thrust is expressed in the same frame using angular coordinates as

$$\mathbf{D} = \begin{pmatrix} D_x \\ D_y \\ D_h \end{pmatrix} = \begin{pmatrix} \sin \theta \cos \psi \\ \sin \psi \\ \cos \theta \cos \psi \end{pmatrix} \quad (5)$$

The angles θ and ψ serve as the thrust direction and attitude coordinates. See Fig. 1. Note that $(\theta, \psi) = (0, 0)$ corresponds to a vertically upward thrust direction. The angles have been defined so that the singularities in the transformation are outside the operating domain.

The dynamics in Cartesian coordinates are

$$\begin{aligned} \dot{x} &= u & \dot{y} &= v & \dot{h} &= w & \dot{u} &= \Gamma \sin \theta \cos \psi \\ \dot{v} &= \Gamma \sin \psi & \dot{w} &= -g + \Gamma \cos \theta \cos \psi & \dot{C} &= \Gamma \end{aligned} \quad (6)$$

In the preceding formulation, we have neglected the dynamics associated with the throttling of the engines and the rotation of the thrust vector. The engines[†] for the MSL lander can be throttled between minimum and maximum thrust in 30–40 ms, and so the thrust magnitude dynamics are very fast compared with the translational and mass dynamics we are considering. For rigidly mounted (nongimbal) engines, the thrust vector is rotated by rotating the lander. For MSL, the maximum attitude rate is 10–15 deg/s [2].

We will consider the attitude motion using the model

$$\dot{\theta} = \omega \quad \dot{\psi} = \nu \quad (7)$$

where the pitch and yaw angular rates are considered to be the controls. We assume the bounds $|\omega| \leq \omega_{\max}$ and $|\nu| \leq \nu_{\max}$. This restricted model for attitude dynamics and control is sufficient to handle boundary conditions on the thrust direction and impose the angular rate limits. The additional complexity of using second-order models for each degree of rotational freedom is not necessary for our purposes in this paper.

[†]Guernsey, C., personal communication, 2005.

By *point-mass model* we mean either the vector form in Eqs. (4) or the coordinate form in Eqs. (6). By *rigid-body model* we mean the combination of the point-mass model and the attitude dynamics in Eqs. (7).

Boundary Conditions

The position and velocity vectors are specified at the initial and final times. The initial conditions are denoted by $\mathbf{r}(0) = \mathbf{r}_0$ and $\mathbf{V}(0) = \mathbf{V}_0$ and the final conditions by $\mathbf{r}(t_f) = \mathbf{0}$ and $\mathbf{V}(t_f) = \mathbf{0}$. The initial conditions are given at the end of the parachute phase; the magnitude of \mathbf{V}_0 is near terminal velocity for the lander/parachute system, in the range 55–90 m/s for MSL [1]. Although we have assumed zero vectors for the final position and velocity, the final altitude could be positive to allow for a final landing maneuver and/or the final vertical velocity could be a small negative nonzero number, without altering the qualitative properties of the minimum-fuel solution. The final time is not specified.

The initial mass is given as $m(0) = m_0$. For the characteristic velocity, the initial condition is $C(0) = 0$. The initial thrust direction is determined by the lander attitude at commencement of the powered descent phase. The thrust vector should be vertically upward at the final time; this is equivalent to specifying that the horizontal acceleration components are zero at the final time. However, the free initial and final thrust direction case will also be considered.

Minimum-Fuel Landing Problems

The performance objective is to minimize propellant usage. This is formulated equivalently as maximizing the final mass of the vehicle (including the remaining propellant) or maximizing $-C(t_f)$. We consider two minimum-fuel landing problems (MFLPs) as indicated in Table 1. In the first (MFLP 1), the point-mass model is used, the controls are assumed to be Γ , θ , and ψ , and the initial and final thrust directions are unspecified (free); in the second (MFLP 2), the rigid-body model is used, the controls are assumed to be Γ , ω , and ν , and the initial and final thrust directions are specified (fixed).

Theoretical Properties of Minimum-Fuel Solutions

In this section, necessary conditions for minimum-fuel solutions are derived and interpreted. The issue of whether a solution exists for a particular problem is not addressed, except to say that a lander can be too far horizontally from the landing site or too close to the surface and going too fast, such that the final boundary conditions cannot be satisfied with any control strategy. Our results parallel those of Meditch [14], who characterized the minimum-fuel solutions for the one-dimensional point-mass model. He derived the first-order necessary conditions using the maximum principle, showed that the minimum-fuel thrust profile is composed of minimum and maximum thrust segments, and is either maximum (max) thrust all the way or a minimum segment followed by a maximum segment (min–max). He also proved that the use of intermediate thrust levels, corresponding to a singular arc, is not optimal. Most of his results regarding the necessary conditions were previously derived by Leitmann [10] using the calculus of variations approach.

MFLP 1: Point-Mass Model with Thrust Angle Control

The cost function to maximize is

$$J = -C(t_f) \quad (8)$$

Table 1 Three minimum-fuel landing problems

MFLP	Model	Controls	Thrust direction	
			Initial	Final
1	point-mass	Γ, θ, ψ	free	free
2	rigid-body	Γ, ω, ν	fixed	fixed

The Hamiltonian associated with the optimal control problem is

$$H(\mathbf{r}, \mathbf{V}, C; \lambda_r, \lambda_v, \lambda_c; \Gamma, \mathbf{D}) = \lambda_r \cdot \mathbf{V} + \lambda_v \cdot (\Gamma \mathbf{D} + \mathbf{g}) + \lambda_c \Gamma \quad (9)$$

where λ_r , λ_v , and λ_c are the costate variables associated with the state variables \mathbf{r} , \mathbf{V} , and C . This problem is a special case of optimal transfer in a uniform gravitational field; the first-order necessary conditions for which are given by Marec ([11], pp. 71–72). According to Pontryagin's maximum principle, the optimal thrust maximizes the Hamiltonian. Let the superscript * denote optimal value. Because Γ is nonnegative, \mathbf{D} should be in the direction of λ_v . Thus, $\mathbf{D}^* = \lambda_v / \lambda_v$. Lawden [8] calls λ_v the *primer vector*. After specifying the thrust acceleration direction, the Hamiltonian can be written as

$$H(\mathbf{r}, \mathbf{V}, C; \lambda_r, \lambda_v, \lambda_c; \Gamma, \mathbf{D}^*) = (\lambda_v + \lambda_c)\Gamma + \lambda_r \cdot \mathbf{V} + \lambda_v \cdot \mathbf{g} \quad (10)$$

which is maximized by

$$\Gamma^* = \begin{cases} \Gamma_{\max} & \text{if } H_\Gamma > 0 \\ \Gamma_{\min} & \text{if } H_\Gamma < 0 \end{cases} \quad (11)$$

where $H_\Gamma = \partial H / \partial \Gamma = \lambda_v + \lambda_c$ is the switching function for Γ . If $H_\Gamma = 0$ over a finite time interval, there is a Γ -singular arc and intermediate thrust levels may be optimal; however, we will show that Γ -singular arcs are not possible.

The costate equations, of the form $\dot{\lambda} = -\partial H^* / \partial x$, where $H^* = H(\mathbf{r}, \mathbf{V}, C; \lambda_r, \lambda_v, \lambda_c; \Gamma^*, \mathbf{D}^*)$ and x denotes the state variable associated with λ , are

$$\dot{\lambda}_r = \mathbf{0} \quad \dot{\lambda}_v = -\lambda_r \quad \dot{\lambda}_c = -(\lambda_v + \lambda_c)k\Gamma^* \quad (12)$$

Because $C(t_f)$ is free, $\lambda_c(t_f) = \partial J / \partial C|_{t=t_f} = -1$. The costate vector λ_r is constant. It follows that $\lambda_v(t) = -\lambda_r(t - t_f) + \lambda_v(t_f)$, where $\lambda_v(t_f)$ is a constant vector to be determined. Thus [11], the thrust vector rotates in a plane in the position space R^3 , the plane containing the origin and the line segment traced out by the tip of the primer vector. Note that if the thrust direction is represented by the angles $[\theta(t), \psi(t)]$, the optimal angles are given by

$$\tan \theta(t) = \frac{\lambda_x(t_f - t) + \lambda_u(t_f)}{\lambda_h(t_f - t) + \lambda_w(t_f)} \quad (13)$$

$$\tan \psi(t) = \frac{\lambda_y(t_f - t) + \lambda_v(t_f)}{\sqrt{[\lambda_x(t_f - t) + \lambda_u(t_f)]^2 + [\lambda_h(t_f - t) + \lambda_w(t_f)]^2}}$$

where the costate vectors are represented by Cartesian coordinates, namely $\lambda_r = (\lambda_x, \lambda_y, \lambda_h)^T$ and $\lambda_v = (\lambda_u, \lambda_v, \lambda_w)^T$. The first of these equations is the tangent steering law that arises in two-dimensional vertical plane powered-flight optimization problems [15]. At a switch time, i.e., at a corner, the costate variables, H^* , and H_Γ are continuous [10].

Because of the translational and rotational symmetries in the problem, there are five integrals (constants) of the motion. Because of the translational position symmetry, the three position costates are constant. The symmetry in time leads to a constant Hamiltonian, and because the final time is free, the Hamiltonian constant is zero. Because of the rotational symmetry around the vertical axis, the vertical component of $\mathbf{r} \times \lambda_r + \mathbf{V} \times \lambda_v$ is constant ([16], pp. 85–86). Because the final position and velocity are zero, this constant is zero. This integral can be written in Cartesian coordinates as

$$(x\lambda_y - y\lambda_x) + (u\lambda_v - v\lambda_u) = 0 \quad (14)$$

Let $\mathbf{p} = [\mathbf{r}^T, \mathbf{V}^T, C; \lambda_r^T, \lambda_v^T, \lambda_c^T]^T$, a 14-dimensional vector, and let $M = \{\mathbf{p} \in R^{14}: f_i(\mathbf{p}) = 0, i = 1, \dots, l\}$ denote the set of points that satisfy the constraints, the constraints specified by l smooth functions $f_i(\mathbf{p})$, $i = 1, \dots, l$. If the vectors $\partial f_i / \partial \mathbf{p}$, $i = 1, \dots, l$ are linearly independent for each $\mathbf{p} \in M$, then M is a smooth $(14 - l)$ -

dimensional manifold [17]. The Hamiltonian integral and the rotational invariance integral imply that extremal solutions (those that satisfy the first-order necessary conditions) lie on a 12-dimensional manifold in the 14-dimensional state–costate space. The extremals can be represented by 13 parameters, one more than the dimension of the manifold because the final time is free.

The length of the velocity costate can be written as

$$\lambda_V(t) = \sqrt{\lambda_r^2(t-t_f)^2 - 2[\lambda_r \cdot \lambda_V(t_f)](t-t_f) + \lambda_V^2(t_f)} \quad (15)$$

There are three cases to consider: 1) with $\lambda_r \neq 0$ and $\lambda_V(t_f) \neq 0$, the graph of $\lambda_V(t)$ is a hyperbola whose major axis is vertical in the (t, λ_V) plane, whose center is at $(t_f + [\lambda_r \cdot \lambda_V(t_f)]/\lambda_r^2, 0)$, and whose curvature is positive; 2) with $\lambda_r \neq 0$ and $\lambda_V(t_f) = 0$, the graph of $\lambda_V(t)$ is a line with (nonzero) negative slope; and 3) with $\lambda_r = 0$ and $\lambda_V(t_f) \neq 0$, the graph of $\lambda_V(t)$ is a line with zero slope, i. e., $\lambda_V(t)$ is constant. First we consider Γ -nonsingular, i. e., bang–bang. For case 1, $\lambda_V(t)$ a hyperbola, the most general form of the optimal Γ profile is max–min–max [10,11]. At a min–max or max–min switch time, $H_\Gamma = 0$ and $\dot{\lambda}_C = 0$. While $\Gamma = \Gamma_{\max}$, $-\dot{\lambda}_C > 0$, and while $\Gamma = \Gamma_{\min}$, $-\dot{\lambda}_C < 0$. Looking at examples of the λ_V and $-\dot{\lambda}_C$ curves in Fig. 2 and noting that at a switch time the curves cross, one can see that the $-\dot{\lambda}_C$ curve can cross the descending $\dot{\lambda}_V < 0$ segment of the λ_V curve at most once and the ascending segment $\dot{\lambda}_V > 0$ at most once. Hence, we conclude the optimal thrust magnitude profile is bang–bang with at most three arcs, two maximum thrust arcs separated by a minimum thrust arc. For case 2, $\lambda_V(t) = -\lambda_r(t-t_f)$. At $t = t_f$, $H^* = (\lambda_V + \lambda_C)\Gamma^* = 0$, which under our assumption of bang–bang control, requires that $\lambda_V(t_f) + \lambda_C(t_f) = 0$. However, this cannot happen, because $\lambda_V(t_f) = 0$ and $\lambda_C(t_f) = -1$. For case 3, $\lambda_r = 0$ implies $\lambda_r = \mathbf{0}$ and from the second of Eqs. (12) we have λ_V constant. Noting, for this case, that $H^* = (\lambda_V + \lambda_C)\Gamma^* + \lambda_V \cdot \mathbf{g} = 0$, that the second term is constant, and that $\text{sign}[\dot{\lambda}_C(t)] = -\text{sign}(H_\Gamma^*)$, one can rule out all bang–bang possibilities except a max–arc. Thus, this is a special case of case 1.

For the singular Γ case, the switching function $H_\Gamma = \lambda_V(t) + \lambda_C(t) = 0$ over a finite time interval. On such an interval, $\dot{\lambda}_C = 0$, hence, λ_C and λ_V are constants. If Γ is singular on any interval, it must be so on the entire interval. Applying the boundary condition on λ_C , we have $\lambda_C = -1$ and $\lambda_V = 1$. Also, $\dot{\lambda}_V = 0$. Differentiating $\lambda_V^2 = \lambda_V \cdot \lambda_V$ and using $\dot{\lambda}_V = -\lambda_r$ from Eqs. (12) yields $\lambda_r \cdot \lambda_V(t) = 0$. Hence λ_r , a constant vector, is orthogonal to $\lambda_V(t)$. A nonzero λ_r would cause the unit-vector $\lambda_V(t)$ to rotate [see the second of Eqs. (12)] and make it impossible for the orthogonality condition to be satisfied over a finite time interval; thus, $\lambda_r = \mathbf{0}$ and λ_V is constant. Using the Hamiltonian integral and the conditions on a singular arc, one can show that the optimal thrust vector, a constant vector, would be orthogonal to \mathbf{g} , i. e., the optimal thrust direction would be in the horizontal plane. We can now rule out the existence of a singular arc, because the vehicle would be in free fall in the vertical direction, making it impossible to satisfy both final conditions $h(t_f) = 0$ and $\dot{h}(t_f) = 0$. Leitmann [10,12] ruled out

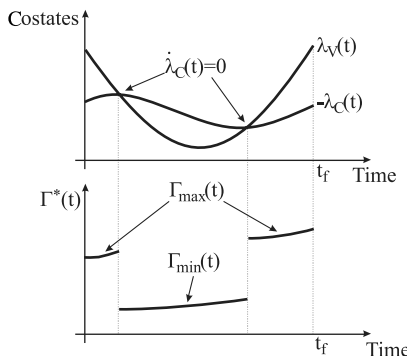


Fig. 2 Example sketch of possible costate behavior and associated switching structure for thrust acceleration magnitude.

singular arcs for the point-mass model for arbitrary boundary conditions and any cost function of the Mayer form. Because our proof relies on particular final conditions, it is not as general, but it is simpler.

Our findings are summarized as follows:

- 1) Singular thrust magnitude arcs do not exist, i. e., using intermediate values of Γ ($\Gamma_{\min} < \Gamma < \Gamma_{\max}$) is never optimal.
- 2) Thrust magnitude is bang–bang:

$$\Gamma^* = \begin{cases} \Gamma_{\max} & \text{if } H_\Gamma > 0 \\ \Gamma_{\min} & \text{if } H_\Gamma < 0 \end{cases}$$

- 3) The optimal Γ^* profile has at most three subarcs, in the order max–min–max.

- 4) There are five integrals for the optimal motion. The three position costates are constant. The Hamiltonian is identically zero, and $(x\lambda_y - y\lambda_x) + (u\lambda_v - v\lambda_u) = 0$. The last two integrals imply that extremal solutions (those that satisfy the first-order necessary conditions) lie on a 12-dimensional manifold in the 14-dimensional state–costate space. The extremals can be represented by 13 parameters, one more than the dimension of the manifold because the final time is free.

MFLP 2: Rigid-Body Model with Angular Velocity Control

For the rigid-body model, we restrict our analysis to the planar case. The planar case is sufficient to explain the features introduced by the attitude dynamics in the numerical solutions presented later, and the analysis is simpler looking in the planar case.

The cost function to maximize is again that given in Eq. (8). We account for the attitude dynamics, but not the cost of controlling them. Boundary conditions are imposed on the pitch angle: $\theta(0) = \theta_0$ and $\theta(t_f) = 0$. The Hamiltonian is

$$H = \lambda_x u + \lambda_h w + \lambda_u \Gamma \sin \theta + \lambda_w (\Gamma \cos \theta - g) + \lambda_C \Gamma + \lambda_\theta \omega \quad (16)$$

The switching functions for the controls Γ and ω are

$$H_\Gamma = \frac{\partial H}{\partial \Gamma} = \lambda_u \sin \theta + \lambda_w \cos \theta + \lambda_C \quad H_\omega = \frac{\partial H}{\partial \omega} = \lambda_\theta \quad (17)$$

and for the nonsingular case, the control laws for maximizing the Hamiltonian are

$$\Gamma^* = \begin{cases} \Gamma_{\max} & \text{if } H_\Gamma > 0 \\ \Gamma_{\min} & \text{if } H_\Gamma < 0 \end{cases} \quad \omega^* = \begin{cases} \omega_{\max} & \text{if } H_\omega > 0 \\ -\omega_{\max} & \text{if } H_\omega < 0 \end{cases} \quad (18)$$

The costate equations are

$$\begin{aligned} \dot{\lambda}_x &= 0 & \dot{\lambda}_h &= 0 & \dot{\lambda}_u &= -\lambda_x & \dot{\lambda}_w &= -\lambda_h \\ \dot{\lambda}_C &= -H_\Gamma \Gamma^* / (g_E I_{sp}) & \dot{\lambda}_\theta &= -\Gamma^* (\lambda_u \cos \theta - \lambda_w \sin \theta) \end{aligned} \quad (19)$$

At a switch time for either Γ or ω , the costate variables, H^* , H_Γ^* , and H_ω^* are continuous.

If $H_\omega = 0$ over a finite time interval, then the control ω is singular on this interval. On an ω -singular arc, we have the conditions

$$\begin{aligned} H_\omega &= \lambda_\theta = 0 & H_\omega^{(1)} &= -\Gamma^* (\lambda_u \cos \theta - \lambda_w \sin \theta) = 0 \\ H_\omega^{(2)} &= -\Gamma^* [(-\lambda_x \cos \theta + \lambda_h \sin \theta) - (\lambda_u \cos \theta - \lambda_w \sin \theta)k] \Gamma^* \\ &\quad + \omega(-\lambda_u \sin \theta - \lambda_w \cos \theta) = 0 \end{aligned} \quad (20)$$

where the superscript (i) denotes the i th derivative with respect to time. These are Lie derivatives, meaning derivatives of scalar functions along the state–costate trajectories. The expression for $H_\omega^{(2)}$ is valid except at the switching times. Thus the ω -singular arc is first-order. On the singular arc, ω is given by

$$\omega = \frac{(-\lambda_x \cos \theta + \lambda_h \sin \theta) - (\lambda_u \cos \theta - \lambda_w \sin \theta)k\Gamma^*}{\lambda_u \sin \theta + \lambda_w \cos \theta} \quad (21)$$

Also, the second of Eqs. (20) implies that the thrust direction is either parallel or antiparallel to the direction of the primer vector $(\lambda_u, \lambda_w)^T$. The generalized Legendre–Clebsch condition

$$-\frac{\partial}{\partial \omega} H_\omega^{(2)} = -\Gamma^*(\lambda_u \sin \theta + \lambda_w \cos \theta) \leq 0 \quad (22)$$

implies that it is necessary that the thrust direction is parallel to the primer vector in order that the singular arc be minimizing. Hence, on an ω -singular arc, the minimizing thrust direction is the direction of the primer vector as it is for the point-mass model.

Next, we prove that Γ -singular arcs are not possible. Because $H_\Gamma = 0$ on a Γ -singular arc, $\lambda_C(t)$ is constant. On an ω -singular arc, the switching function for the thrust magnitude is $H_\Gamma = \lambda_V + \lambda_C$, where $\lambda_V = (\lambda_u^2 + \lambda_w^2)^{1/2}$, the same form, Eq. (15), it has for the point-mass model. Therefore, the proof given earlier, showing that Γ cannot be singular, is valid on a singular arc for the rigid-body model. Now consider an ω -nonsingular arc. Differentiating

$$H_\Gamma^* = \lambda_u \sin \theta + \lambda_w \cos \theta + \lambda_C = 0 \quad (23)$$

along an extremal (taking a Lie derivative) yields

$$H_\Gamma^{*(1)} = -\lambda_x \sin \theta - \lambda_h \cos \theta + (\lambda_u \cos \theta - \lambda_w \sin \theta)\omega^* = 0 \quad (24)$$

Differentiating again we obtain

$$H_\Gamma^{*(2)} = [-2(\lambda_x \cos \theta - \lambda_h \sin \theta) + \lambda_C \omega^*]\omega^* = 0 \quad (25)$$

except at switch times. Because (λ_x, λ_h) is constant and ω^* is piecewise constant and nonzero, $H_\Gamma^{*(2)} = 0$ implies that θ is piecewise constant. But this contradicts $\dot{\theta} = \omega^* \neq 0$. Thus, we can rule out Γ singular in the ω -nonsingular case.

From a geometric perspective, the 12-dimensional state–costate space for the planar rigid-body minimum-fuel problem is reduced to an 11-dimensional manifold by the Hamiltonian integral, $H^* = 0$. The singular manifold, composed of the state–costate points that satisfy the first two of Eqs. (20), is a nine-dimensional submanifold of the 11-dimensional manifold. On the singular manifold, Γ^* and θ^* are specified by the same control laws for the rigid-body problem as they are for the point-mass problem. With the initial and final values of θ^* free, the extremal solution for the rigid-body model will lie on the singular manifold and be the same as that for the point-mass model, provided that the bound $|\dot{\theta}^*| \leq \omega_{\max}$ imposed for the rigid-body model is not exceeded. With boundary conditions on θ , such that the thrust is not in the direction of the primer vector at the initial and final times, the extremal trajectory will begin and end off the singular manifold. Whether it will lie on the singular manifold in between depends on how fast the attitude dynamics are relative to the point-mass dynamics and the degree of separation between the boundary conditions. This is a qualitative characterization. In the next section, we compare solutions for the point-mass model and the rigid-body model illustrating that they can be similar or different, depending on the boundary conditions.

Numerical Solutions for Minimum-Fuel Landing

Solution Method

Numerical solutions of the minimum-fuel landing problems are obtained using the graphical environment for simulation and optimization (GESOP) software. GESOP approximates an optimal control problem by a parameter optimization problem, i.e., a nonlinear programming (NLP) problem, and then solves the NLP problem. Of the two options provided for approximating an optimal control problem as an NLP problem, we chose the direct collocation method, trajectory optimization by direct collocation.

Table 2 Initial conditions for the two study cases

	Case 1	Case 2
x_0 , m	1900	1900
y_0 , m	0	0
h_0 , m	3100	3100
u_0 , m/s	40	0
v_0 , m/s	0	40
w_0 , m/s	-50	-50

The resulting approximation for the optimal control problem is an NLP problem of the form

$$\min J(\mathbf{q}) \quad (26)$$

subject to

$$c_i(\mathbf{q}) = 0, \quad i = 1, \dots, n_{ec} \quad (27)$$

$$c_i(\mathbf{q}) \leq 0, \quad i = n_{ec} + 1, \dots, n_c \quad (28)$$

where \mathbf{q} is the vector of parameters, c_i , $i = 1, \dots, n_c$ are the constraint functions, n_c is the total number of the constraints, n_{ec} is the number of equality constraints, and $n_c - n_{ec}$ is the number of inequality constraints. GESOP provides sequential quadratic programming based NLP-solvers; of these we chose SNOPT [18].

In GESOP, the integration error and the optimization tolerance can be specified by the user. The optimization tolerance determines how accurately the Karush–Kuhn–Tucker conditions are satisfied. We used an optimization tolerance of 10^{-6} . The integration error was set at 10^{-8} . The user also specifies the number and location of the nodes for the discretization. We used 70 evenly spaced nodes from 0 to t_f initially to estimate where the switch times occur for the bang–bang controls. Extra nodes were added around the switch times. Then another optimization was run. The extra nodes improved the accuracy of the switch times, but introduced artificial high-frequency oscillations, especially in the angular velocity controls. Further manual adjustment of some node positions and reoptimization essentially eliminated the high-frequency oscillations.

Solutions

Solutions for two sets of initial conditions (see Table 2) are shown in position space in Fig. 3 and in more detail in later figures. The vehicle model is similar to those used in other studies [2,6] and is representative of the MSL lander. For the numerical solutions, mass rather than characteristic velocity is used as a state variable, and throttle is used as the control rather than specific thrust magnitude. The throttle setting τ is allowed to vary between 0.3 and 0.8 and the effective thrust used in the equations of motion is computed by

$$T = \tau T_{\text{total}} \cos \beta \quad (29)$$

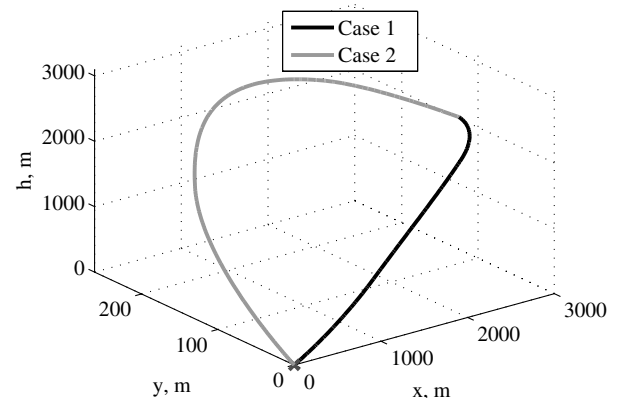


Fig. 3 Position coordinates for the two study cases.

**<http://www.gesop.de>

where $T_{\text{total}} = 16,423$ N is the combined thrust of all the engines and $\beta = 0.4712$ rad (equivalent to 27 deg) is the cant angle for the engines. The initial mass of the vehicle is $m(0) = m_V + m_F(0)$ where $m_V = 1505$ kg and $m_F(0) = 400$ kg are, respectively, the mass of the vehicle without propellant and the propellant mass. The mass change equation is

$$\dot{m} = -\frac{1}{g_E I_{\text{sp}}} \tau T_{\text{total}} \quad (30)$$

where $I_{\text{sp}} = 225$ s and $g_E = 9.807$ m/s². The introduction of multiple engines and the cant angle and using the throttle as the control variable do not invalidate any of the results from the preceding section; it was necessary to compare fuel consumption numbers with those from other studies. For MFLP 2 (rigid-body), the pitch and yaw rates are constrained by $-\omega_{\text{max}} \leq \omega \leq \omega_{\text{max}}$ and $-\nu_{\text{max}} \leq \nu \leq \nu_{\text{max}}$. We use $\omega_{\text{max}} = \nu_{\text{max}} = 10$ deg/s.

To check the accuracy of the GESOP solutions, we compared the analytical solution for the 1 degree-of-freedom minimum-fuel vertical descent problem [14] to the numerical solution for MFLP 1 obtained via GESOP for the following initial conditions. The vehicle starts directly over the landing site with zero horizontal velocity, $h_0 = 3100$ m and $w_0 = -50$ m/s. In the numerical solution, the thrust is directed vertically upward always [$\theta(t) \equiv 0$; $\psi(t) \equiv 0$] and a min-max thrust profile is used. The numerical solution closely agrees with the analytical solution as indicated by the following comparisons to the switching time, final time, and propellant mass consumption. The values of these variables are rounded to three decimal points. We used 500 nodes to compute the numerical solution. The switching times for the analytical and GESOP solutions are 29.682 and 29.721 s, respectively (0.131% error).

Furthermore, the final times for the analytical and GESOP solutions are 56.183 and 56.181 s, respectively (0.004% error). Finally, the propellant mass consumptions are 213.135 and 213.126 kg, respectively (0.004% error).

Case 1, Figs. 4 and 5

The vehicle is initially 1900 m downrange, 3100 m above the surface, and heading away from the landing site. Examining the solution for MFLP 1, there is no crossrange motion in the optimal descent [$y(t) \equiv 0$, $v(t) \equiv 0$]. The optimal thrust profile is max-min-max. The thrust always has a positive vertical component to manage the descent rate, i.e., $-90 \text{ deg} < \theta(t) < 90 \text{ deg}$. Initially there is a significant negative horizontal thrust component to reverse the horizontal velocity component u from 40 to -40 m/s, so that the vehicle is heading toward the landing site. During the period from 12–32 s, minimum thrust is used and the pitch angle transitions from negative to positive values. The last phase of the trajectory is flown with maximum thrust and positive pitch angle to bring the horizontal velocity to zero by the time the vehicle reaches the landing site. For MFLP 2, we compute the solutions for the same boundary conditions used for MFLP 1, except for the addition of thrust direction constraints $\theta(0) = -40$, $\psi(0) = 0$, $\theta(t_f) = 0$, and $\psi(t_f) = 0$ deg. There are maximum rate pitch maneuvers to transition from the pitch angle boundary condition to the pitch angle for the primer vector and vice versa. Because the boundary layers for MFLP 2 are brief, the solution is similar to that of MFLP 1. The most noticeable differences are the switch times for the throttle. The propellant mass consumed Δm is 263.4 kg for MFLP 1. Accounting for the angle boundary conditions, attitude dynamics, and angular velocity constraints in MFLP 2 only increased the fuel required by 1.20% (i.e., the fuel consumption is 3.16 kg greater for MFLP 2).

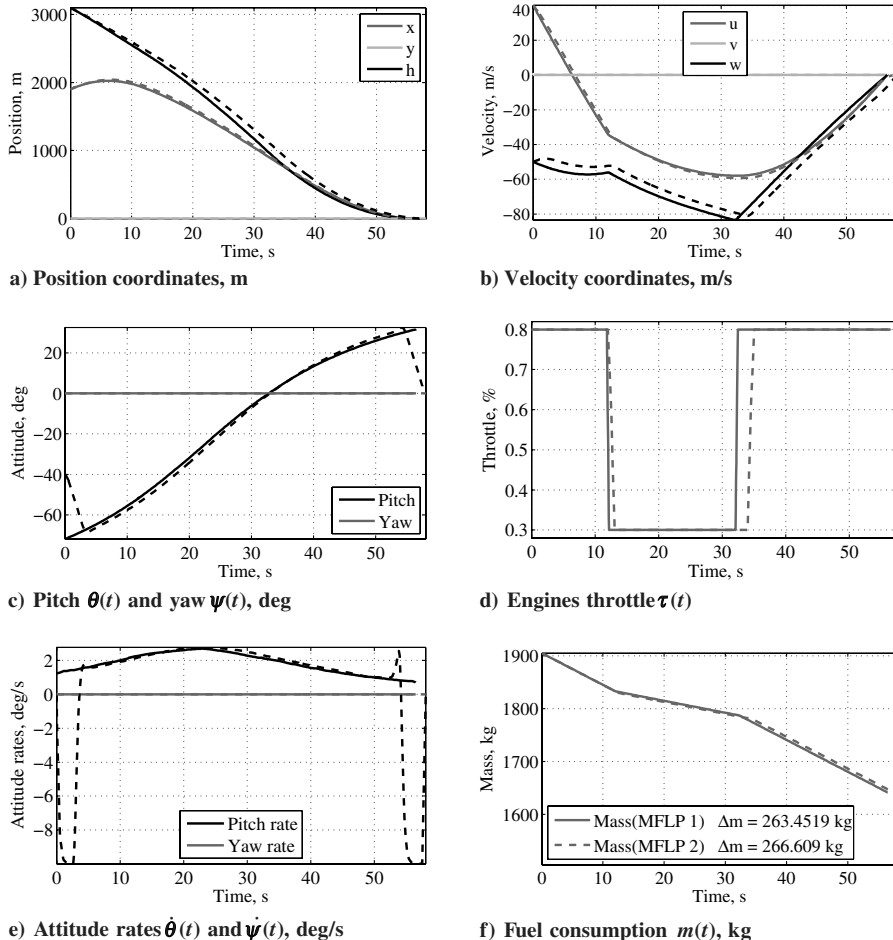


Fig. 4 Solutions for MFLP 1 (solid line) and MFLP 2 (dashed line) for case 1: vehicle initially heading 180 deg away from site (essentially a two-dimensional problem) with -40 deg initial pitch angle.

For Case 1, we have increased the angular rate limit to 20 deg/s and have seen that the boundary layers are shorter in duration and the singular arc solution matches more closely the point-mass solution. With a 10 deg/s limit, the differences in the Γ switch times (relative to the solution for MFLP 1) are less than 1 s; for a 20 deg/s limit, the delays are less than 0.5 s. We note that the node spacing for the numerical solutions is 0.15 s, so that even in the unconstrained case it takes this much time to switch between thrust limits.

The solutions portrayed in Fig. 5 are for the same problems considered for Fig. 4 except that, for MFLP 2, the initial pitch angle, $\theta(0) = 60$ deg, is considerably farther from the pitch angle (-70 deg) for the primer vector. Because the thrust is initially in an ineffective direction, minimum throttle is used until the thrust vector is rotated to closer alignment with the primer vector. The horizontal distance from the landing site increases beyond what was seen in Fig. 4 while the pitch angle is adjusted. The overall throttle profile is thus min-max-min-max and the max to min and second min to max switch times are significantly different. The flight time is 10 s longer. The fuel consumption is 15.73% greater for the MFLP 2 problem. Thus, Figs. 4 and 5 illustrate that the solutions for the point-mass and rigid-body models can be very similar or very different, depending on the boundary conditions for the pitch angle relative to the primer vector pitch angle. A nonzero initial condition for ψ would similarly require an initial boundary-layer yaw maneuver to transition to the yaw angle for the primer vector, which is identically zero for this case.

Case 2, Fig. 6

The vehicle is initially heading in the crossrange direction, making this a three-dimensional case. For MFLP 1, a nonzero yaw component of thrust is used to drive the crossrange velocity component to zero over the course of the trajectory. The optimal

throttle profile is max-min-max. For MFLP 2, there are initial and final boundary-layer transitions to and from the singular manifold to satisfy the boundary conditions on θ and ψ , which are $\theta(0) = -40$, $\psi(0) = -20$, $\theta(t_f) = 0$, and $\psi(t_f) = 0$ deg. Because the boundary layers are brief, most of the solution is an ω -singular arc and matches closely the solution for MFLP 1. The propellant mass consumed Δm is 241.45 kg for MFLP 1. Adding the constraints of MFLP 2 only increased the fuel required by 0.80% (i.e., the fuel consumption is 1.93 kg greater for MFLP 2). With larger initial θ and ψ offsets from the values consistent with the primer vector, there would be larger differences in the solutions for MFLP 1 and MFLP 2.

Conclusions

Motivated by the requirement for pinpoint landing in future Mars missions, we considered the problem of minimum-fuel powered terminal descent to a prescribed landing site. The first-order necessary conditions were derived and interpreted for a point-mass model with throttle and thrust angle control and for a rigid-body model with throttle and angular velocity control, clarifying the characteristics of the minimum-fuel solution in each case. The optimal thrust magnitude profile is bang-bang for both models; for the point-mass, the most general thrust magnitude profile has a max-min-max structure. The optimal thrust direction law for the point-mass model (alignment with the primer vector) corresponds to a singular solution for the rigid-body model. Whether the point-mass solution accurately approximates the rigid-body solution depends on the thrust direction boundary conditions imposed for the rigid-body model. Minimum-fuel solutions, obtained numerically, illustrated the optimal strategies.

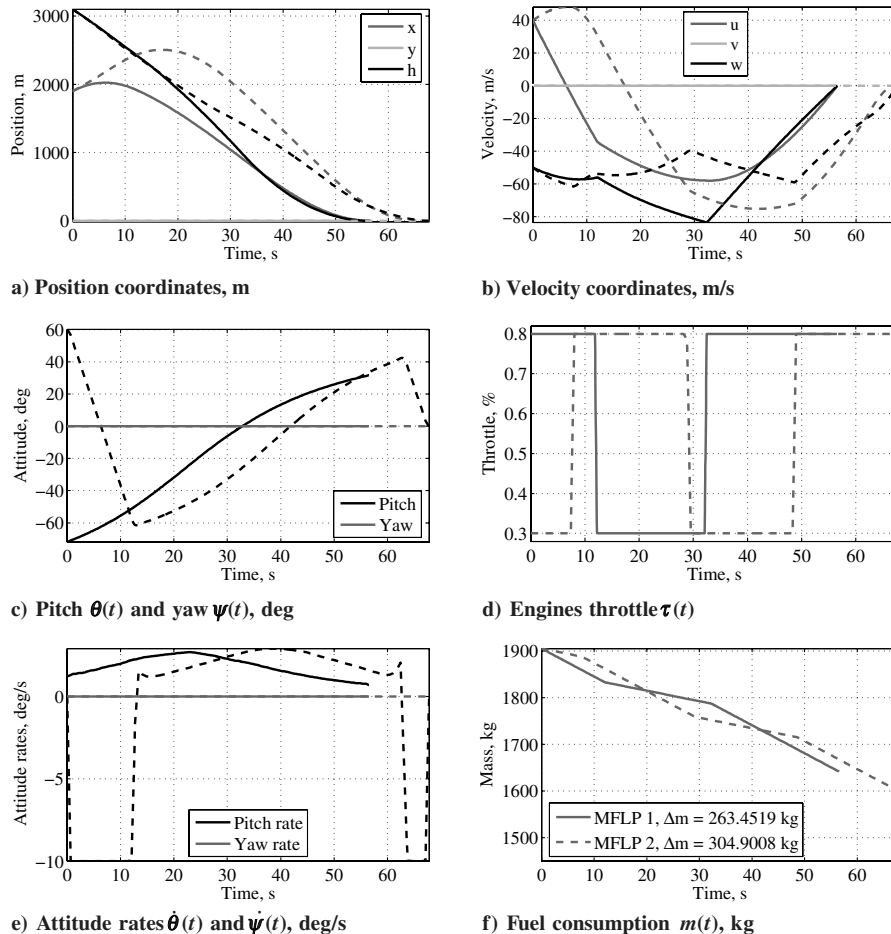


Fig. 5 Solutions for MFLP 1 (solid line) and MFLP 2 (dashed line) for case 1: vehicle initially heading 180 deg away from site (essentially a two-dimensional problem) with an initial pitch angle of 60 deg.

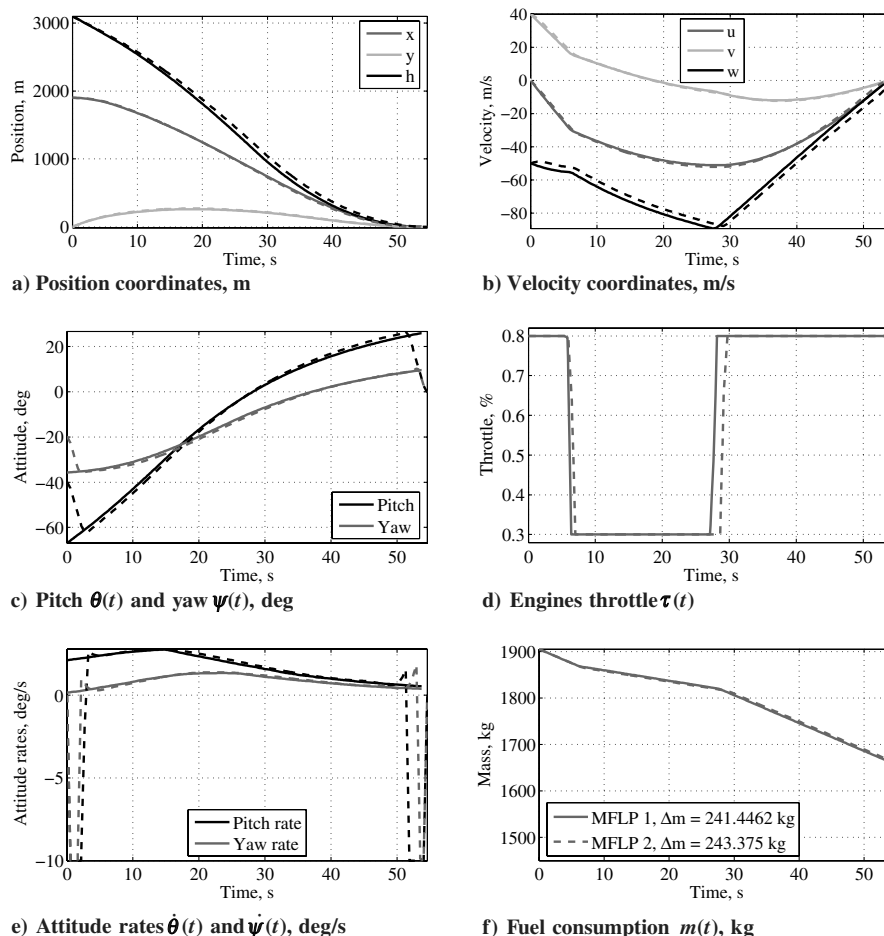


Fig. 6 Solutions for MFLP 1 (solid line) and MFLP 2 (dashed line) for case 2: vehicle initially heading 90 deg away from direction of site (a three-dimensional problem) with initial pitch and yaw angles of -40 and -20 deg, respectively.

Acknowledgments

The research described in this paper was supported by the Jet Propulsion Laboratory, California Institute of Technology, under contract with NASA. Helpful discussions with A. A. Wolf, W. R. Johnson, A. B. Acikmese, and S. R. Ploen of the Jet Propulsion Laboratory are gratefully acknowledged.

References

- [1] Braun, R. D., and Manning, R. M., "Mars Exploration Entry, Descent and Landing Challenges," Institute of Electrical and Electronics Engineers (IEEE) Conf. Paper AERO.2006.1655790, 2006.
- [2] Wong, E. C., Singh, G., and Masciarelli, J. P., "Guidance and Control Design for Hazard Avoidance and Safe Landing on Mars," *Journal of Spacecraft and Rockets*, Vol. 43, No. 2, 2006, pp. 378–384.
- [3] Klump, A. R., "Apollo Lunar Descent Guidance," *Journal of Guidance, Control, and Dynamics*, Vol. 10, No. 2, 1974, pp. 133–146.
- [4] Sostaric, R. R., and Rea, J. R., "Powered Descent Guidance Methods for the Moon and Mars," *AIAA Guidance, Navigation, and Control Conference and Exhibit*, AIAA Paper 2005-6287, 2005.
- [5] D'Souza, C. N., "Optimal Guidance Law for Planetary Landing," *AIAA Guidance, Navigation, and Control Conference and Exhibit*, AIAA Paper 1997-3709, 1997.
- [6] Acikmese, A. B., and Ploen, S. R., "Powered Descent Guidance Algorithm for Mars Pinpoint Landing," *AIAA Guidance, Navigation, and Control Conference and Exhibit*, AIAA Paper 2005-6288, 2005.
- [7] Najson, F., and Mease, K. D., "Computationally Non-Expensive Guidance Algorithm for Fuel Efficient Soft Landing," *Journal of Guidance, Control, and Dynamics*, Vol. 29, No. 4, 2006, pp. 955–964.
- [8] Lawden, D. F., *Optimal Trajectories For Space Navigation*, Butterworths, London, 1963.
- [9] Miele, A., "Calculus of Variations in Applied Aerodynamics and Flight Mechanics," *Optimization Techniques with Applications to Aerospace Systems*, edited by G. Leitmann, Academic Press, New York, 1962.
- [10] Leitmann, G., "Class of Variational Problems in Rocket Flight," *Journal of the Aero/Space Sciences*, Vol. 26, No. 9, 1959, pp. 586–591.
- [11] Marec, J. P., *Optimal Space Trajectories*, Elsevier, New York, 1979.
- [12] Leitmann, G., "Variational Problems with Bounded Control Variables," *Optimization Techniques with Applications to Aerospace Systems*, edited by G. Leitmann, Academic Press, New York, 1962.
- [13] Kelley, H. J., "Boundary-Layer Approximation to Powered-Flight Attitude Transients," *Journal of Spacecraft and Rockets*, Vol. 7, July 1970, p. 879.
- [14] Meditch, J., "On the Problem of Optimal Thrust Programming for a Lunar Soft Landing," *IEEE Transactions on Automatic Control*, Vol. 9, No. 4, 1964, pp. 477–484.
- [15] Lawden, D., "Optimal Rocket Trajectories," *ARS Journal*, Vol. 27, No. 12, 1957, pp. 22–27.
- [16] Vinh, N. X., *Optimal Trajectories in Atmospheric Flight*, Elsevier, New York, 1981.
- [17] Isidori, A., *Nonlinear Control Systems*, 2nd ed., Springer-Verlag, New York, 1989.
- [18] Gill, P. E., Murray, W., and Saunders, M. A., "SQP Algorithm for Large Sparse Optimization," Univ. of California, TR NA 95-0, Dept. of Mathematics, San Diego, CA, 1995.

C. McLaughlin
Associate Editor